Effects of Ti3C2Tx MXene Addition to a Co Complex/Ionic Liquid-Based Electrolyte on the Photovoltaic Performance of Solar Cells

Ju Hee Gu , Dongho Park , Kyung-Hye Jung , Byung-Chul Lee , Yoon Soo Han *

Posted Date: 21 February 2024

doi: 10.20944/preprints202402.1201.v1

Keywords: dye-sensitized solar cell; redox mediator; Ti3C2Tx MXene; hole conduction

Article

Effects of Ti_3C_2Tx MXene Addition to a Co Complex/Ionic Liquid-Based Electrolyte on the Photovoltaic Performance of Solar Cells

Ju Hee Gu, Dongho Park, Kyung-Hye Jung, Byung-Chul Lee and Yoon Soo Han *

Department of Advanced Materials and Chemical Engineering, Daegu Catholic University, Gyeongbuk 38430, Republic of Korea; gjh3170@naver.com (J.H.K.); donggeulhonyang@naver.com (D.P.); khjung@cu.ac.kr (K.-H.J.); bclee@kbsc.ac.kr (B.-C.L.)

* Correspondence: yshancu@cu.ac.kr

Abstract: Redox mediators comprising I^-, **Co^{3+}, and** Ti_3C_2Tx MXene were applied to dye-sensitized solar cells (DSCs). In the as-prepared DSCs (I-DSCs), wherein hole conduction occurred via the redox reaction of I^-/I_3^- ions, the power conversion efficiency (PCE) was not altered by the addition of Ti_3C_2Tx MXene. The I-DSCs were exposed to light to produce Co^{2+}/Co^{3+}-based cells (Co-DSCs), wherein the holes were transferred via the redox reaction of Co^{2+}/Co^{3+} ions. A PCE of 9.01% was achieved in a Co-DSC with Ti_3C_2Tx MXene (Ti_3C_2Tx-Co-DSC), which indicated an improvement from the PCE of a bare Co-DSC without Ti_3C_2Tx MXene (7.27%). It was also found that the presence of Ti_3C_2Tx MXene in the redox mediator increased the hole collection, dye regeneration, and electron injection efficiencies of the Ti_3C_2Tx-Co-DSC, leading to an improvement in both the short-circuit current and the PCE when compared with those of the bare Co-DSC without MXene.

Keywords: dye-sensitized solar cell; redox mediator; Ti_3C_2Tx MXene; hole conduction

1. Introduction

Two-dimensional (2D) materials are typically crystalline solids consisting of a single layer of atoms. These materials are considered promising for various applications, which explains why they remain the focus of research. MXenes with a general formula of $M_{n+1}X_nT_x$ (where n = 1–3; M denotes a transition metal; X is either carbon or nitrogen; and T_x indicates surface terminal groups such as –OH, –F, –Cl, and/or –O–) were created by selectively etching the "A" layers from layered MAX phases ($M_{n+1}AX_n$, where A is usually any element from among Cd, Al, Si, P, S, Ga, Ge, As, In, Sn, Tl, Pb, and S [groups 12–16]) and can be easily solution-processed in aqueous or polar organic solvents due to their hydroxyl- or oxygen-terminated surfaces [1–4]. Following the production of multilayered Ti_3C_2Tx MXene by etching the Al layers from the Ti_3AlC_2 MAX phase in 2011 at Drexel University [1], numerous related research results have been reported in the fields of energy storage, sensors, light-emitting diodes, electromagnetic shielding, and environmental applications [2–4]. In addition, MXenes have been extensively studied in relation to applications concerning solar cells, given their metallic conductivity, excellent charge carrier mobility, high optical transmittance, and tunable work function [5–8]. Among the various MXenes, $Ti_3C_2T_x$ is the most commonly studied in terms of third-generation solar cells, such as dye-sensitized solar cells (DSCs) [9–11], perovskite solar cells [12–14], and polymer solar cells [15,16]. A conventional DSC is composed of a dye-adsorbed TiO_2 layer on a transparent electrode (i.e., a working electrode), a liquid electrolyte, and a Pt catalytic layer on a conductive electrode (i.e., a Pt counter electrode). Light absorption in dye molecules leads to the formation of excitons (electron–hole pairs), and the excited electrons are injected into the TiO_2 layer. The photoinjected electrons and the holes in the dye molecules are transported to the electrodes via the TiO_2 layer and the electrolyte, respectively. Finally, the electrons and holes are collected in the electrodes, allowing electron flows through the external circuits to occur [17,18]. The hole-conducting electrolyte is comprised of redox couples and electrical additives [19,20]. The redox couples, such as I^-/I_3^-, Co^{+2}/Co^{+3}, Cu^{+1}/Cu^{+2}, and Ni^{+3}/Ni^{+4}, are reduced near the Pt counter electrode and oxidized near

 doi:10.20944/preprints202402.1201.v1

the excited dye molecules, thereby allowing for hole collection and dye regeneration, respectively. Electrical additives such as 4-tert-butylpyridine (TBP) and cations (lithium [Li^+] or guanidinium [$C(NH_2)^{3+}$]) represent another important ingredient in a liquid electrolyte for enhancing the photovoltaic parameters of cells. These additives can control the potential of the redox couple, the surface state of the TiO_2 semiconductor, the shift in the conduction band edge, and the interfacial charge recombination through being incorporating in small amounts [20]. $Ti_3C_2T_x$ MXene was introduced as an additive for electrolytes to improve the photovoltaic performance of quasi-solid-state DSCs [21,22]. Sun et al. reported that, via the addition of $Ti_3C_2T_x$ MXene to a quasi-solid-state electrolyte composed of an I^-/I_3^- redox couple and a melamine-formaldehyde (MF) sponge, the average power conversion efficiency (PCE) of the DSCs under a room light condition (1000 lux) was improved by 26.92% from that of the reference cell without MXene (23.35%) [21]. It was also reported that a PCE of 29.94% under a condition of 1000 lux was achieved through the incorporation of both reduced graphene oxide and $Ti_3C_2T_x$ to a quasi-solid-state electrolyte containing an I^-/I_3^- redox couple, polyethylene oxide (PEO), and poly(vinylidene fluoride-co-hexafluoropropylene) (PVDF-HFP) [22].

In this study, we report the effects of $Ti_3C_2T_x$ MXene addition to a liquid electrolyte on the photovoltaic performance of cells. $Ti_3C_2T_x$-dispersed liquid electrolytes based on a metal complex (tris(2-(1*H*-pyrazol-1-yl)-4-tert-butylpyridine)cobalt(III) tri[bis(trifluoromethane)sulfonimide] [FK209]) as a source of Co^{3+} and an ionic liquid (1-methyl-3-propylimidazolium iodine [MPII]) as a source of I^- (iodide) were first prepared. Then, DSCs with $Ti_3C_2T_x$-dispersed Co^{3+}/I^- liquid electrolytes (redox mediators) were fabricated and their photovoltaic properties were compared with those of the reference cell without $Ti_3C_2T_x$ MXene. To the best of our knowledge, this is the first report on the effects of $Ti_3C_2T_x$ addition to Co complex (Co^{3+})/ionic liquid (I^-)-based redox mediators. The reported photovoltaic parameters (short-circuit current [J_{sc}], open-circuit voltage [V_{oc}] and fill factor [*FF*]) of the DSCs with $Ti_3C_2T_x$ MXene are summarized in Table 1, including those of our devices with FK209 (Co^{3+})/MPII (I^-)/$Ti_3C_2T_x$-based liquid electrolytes.

Table 1. Photovoltaic performances of DSCs with $Ti_3C_2T_x$-MXene-incorporated electrolytes.

Device	Measurement condition	Redox mediator		J_{sc} (mA/cm²)	V_{oc} (V)	*FF* (%)	**PCE** (%)	Ref.
Quasi-solid-state DSC	AM 1.5	MF-sponge-based I^-/I_3^-	Without Ti_3C_2Tx	14.979 ± 0.175	0.778 ± 0.004	65.3 ± 0.3	7.610 ± 0.106	[21]
			With Ti_3C_2Tx	15.085 ± 0.188	0.781 ± 0.003	66.4 ± 0.6	7.822 ± 0.092	[21]
	1000 lux	MF-sponge-based I^-/I_3^-	Without Ti_3C_2Tx	0.177 ± 0.001	0.569 ± 0.007	70.3 ± 0.5	23.35 ± 0.43	[21]
			With Ti_3C_2Tx	0.196 ± 0.003	0.579 ± 0.004	71.9 ± 0.4	26.92 ± 0.43	[21]
	AM 1.5	PEO/PVDH-HFP-based I^-/I_3^-	Without rGO/Ti_3C_2Tx	-	-	-	-	-
			With rGO/Ti_3C_2Tx	15.170 ± 0.203	0.783 ± 0.002	69.5 ± 0.5	8.255 ± 0.109	[22]
	1000 lux	PEO/PVDH-HFP-based I^-/I_3^-	Without Ti_3C_2Tx	-	-	-	-	-
			With rGO	0.189 ± 0.002	0.544 ± 0.002	76.1 ± 0.4	23.22 ± 0.43	[22]
			With rGO/Ti_3C_2Tx	0.223 ± 0.001	0.561 ± 0.004	75.7 ± 0.1	29.94 ± 0.49	[22]
Liquid-electrolyte DSC	AM 1.5	Co^{3+}/ I^- (FK209/MPII)	Without Ti_3C_2Tx	15.46 ± 1.04	0.760 ± 0.023	61.33 ± 3.70	7.18 ± 0.11	This study
			With Ti_3C_2Tx	18.09 ± 0.94	0.746 ± 0.014	63.66 ± 2.69	8.58 ± 0.30	This study

2. Results and Discussion

 doi:10.20944/preprints202402.1201.v1

2.1. Photovoltaic Performance of DSCs Based on $Ti_3C_2T_x$-Incorporated Co^{3+}/I^- Redox Mediators

In a previous report, we revealed that, through the simple mixing of MPII and FK209, triiodide (I_3^-) and Co^{2+}(FK209) were produced via a chemical reaction (1) between the iodide (I^-) of MPII and Co^{3+}(FK209), where Co^{2+}(FK209) and Co^{3+}(FK209) are the Co^{2+} and Co^{3+} ions of FK209, respectively. Since the Co^{3+}(FK209) was almost fully converted into Co^{2+}(FK209), the redox mediators contained both I_3^- and Co^{2+}(FK209) as well as I^- (originating from non-reacted MPII) [23]. Therefore, hole conduction occurs through reactions (2)–(5) when as-prepared DSCs are exposed to the AM 1.5 condition, indicating that the I^-/I_3^- redox couple is involved in the dye regeneration (reaction [4]) and hole collection (reaction [5]). Here, we code the as-prepared DSCs based on the I^-/I_3^- redox couple as I-DSCs.

$$3I^- + 2Co^{3+}(FK209) \rightarrow I_3^- + 2Co^{2+}(FK209) \quad (1)$$
$$2Dye + h\nu \rightarrow 2Dye^* \quad (2)$$
$$2Dye^* \rightarrow 2Dye^+ + 2e^- (TiO_2) \quad (3)$$
$$3I^- + 2Dye^+ \rightarrow I_3^- + 2Dye \quad (4)$$
$$I_3^- + 2e^- (Pt) \rightarrow 3I^- \quad (5)$$

Using the FK209 (Co^{3+})/MPII (I^-) redox mediators with or without $Ti_3C_2T_x$ MXene, DSCs were fabricated and the variations in the photovoltaic parameters were investigated. The average photovoltaic performance measured using the four I-DSCs (i.e., the as-prepared DSCs) are compared in Figure 1 and Table 2, while the raw data are presented in Table S1 in the electronic supplementary information (ESI). Through the incorporation of $Ti_3C_2T_x$ MXene into the Co^{3+}/I^- liquid redox mediators, the average J_{sc} value of the I-DSCs was enhanced, whereas the average V_{oc} value was decreased when compared with the values of the device without MXene, as shown in Figure 1a,b, respectively. As a result, the average PCE of the I-DSCs with $Ti_3C_2T_x$ was very similar to that of the cells without $Ti_3C_2T_x$.

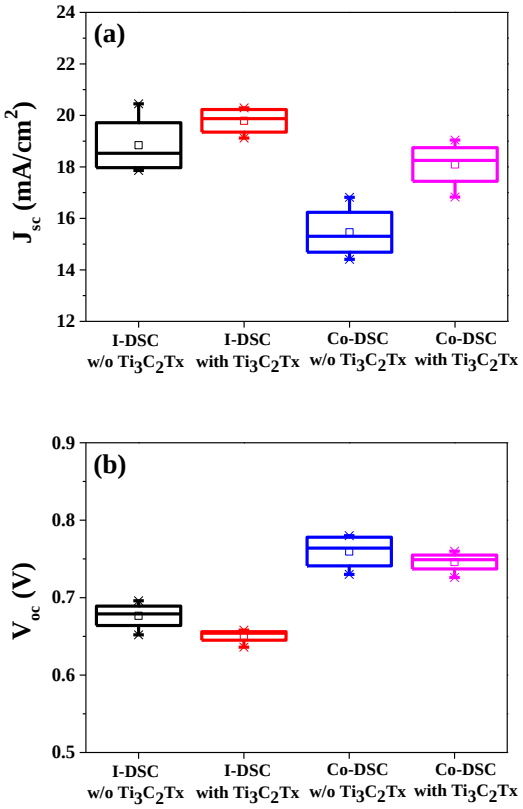

Preprints.org (www.preprints.org) | NOT PEER-REVIEWED | Posted: 21 February 2024 doi:10.20944/preprints202402.1201.v1

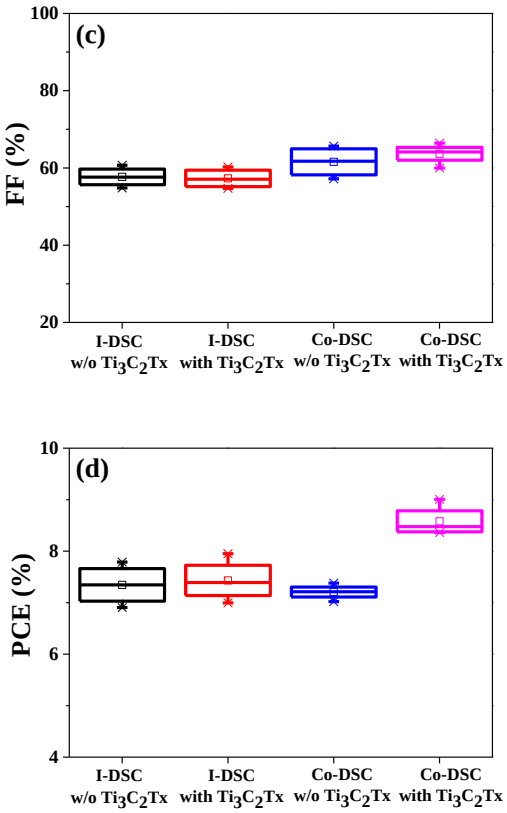

Figure 1. Performance comparison of the I- and Co-DSCs with or without $Ti_3C_2T_x$ MXene: (a) J_{sc}, (b) V_{oc}, (c) *FF*, and (d) PCE measured under AM 1.5 irradiation.

Table 2. Averages and standard deviations of the cell performances measured using four I- and Co-DSCs with or without $Ti_3C_2T_x$ MXene.

	Devices	J_{sc} (mA/cm²)	V_{oc} (V)	*FF* (%)	PCE (%)
I-DSC	Without $Ti_3C_2T_x$	18.84 ± 1.18	0.677 ± 0.018	57.70 ± 2.55	7.35 ± 0.39
	With $Ti_3C_2T_x$	19.95 ± 0.78	0.651 ± 0.010	57.29 ± 2.59	7.43 ± 0.40
Co-DSC	Without $Ti_3C_2T_x$	15.46 ± 1.04	0.760 ± 0.023	61.33 ± 3.70	7.18 ± 0.11
	With $Ti_3C_2T_x$	18.09 ± 0.94	0.746 ± 0.014	63.66 ± 2.69	8.58 ± 0.30

Moreover, it was also found that chemical reactions (6) and (7) occurred through the exposure of the I-DSCs to light for a certain time [23]. Under illumination, the Co^{2+}(FK209) that was produced via reaction (1) reduced the oxidized dye (Dye^+), thereby regenerating Co^{3+}(FK209) at the dye/redox mediator interface (reaction [6]). The resulting Co^{3+}(FK209) diffused to the counter electrode and then reduced to Co^{2+}(FK209) through receiving an electron from the platinized FTO electrode (reaction [7]), indicating that the Co^{2+}/Co^{3+} redox couple is related to the dye regeneration (reaction [6]) and hole collection (reaction [7]). This may lead to an increase in the V_{oc} value of the Co^{2+}/Co^{3+}-based cell when compared with that of the I^-/I_3^--based cell, as the potential gap between the conduction band edge (CBE) of the TiO_2 and the redox potential (1.06 V *versus* a normal hydrogen electrode [NHE]) of the Co^{2+}/Co^{3+}(FK209) is wider than that (0.35 V *versus* a NHE) of the I^-/I_3^- electrolyte [24–26]. Here, we code the DSCs based on the Co^{2+}/Co^{3+} redox couple as Co-DSCs, which were transformed from the I-DSCs via exposure to AM 1.5 light. To determine the time taken to convert the I-DSCs into Co-DSCs, we measured the V_{oc} variations with the light-exposure time of the I-DSCs. As shown in Figure S1, the V_{oc} values improved with an increasing exposure time and then saturated after over a period of 150 min. This indicates that hole conduction mainly occurred through the action of the Co^{2+}/Co^{3+}

 doi:10.20944/preprints202402.1201.v1

redox couple after exposure of the I-DSCs to light for over 150 min. To investigate effects of the MXene incorporation in Co-DSCs, the I-DSCs with or without $Ti_3C_2T_x$ MXene were exposed to AM 1.5 condition for 150 min and their photovoltaic performance was measured. As a reference, the V_{oc} values of the Co-DSCs was sharply increased when compared with those of the I-DSCs due to the wider potential gap between the TiO_2's CBE and the Co^{2+}/Co^{3+}(FK209)'s redox potential, as mentioned above. This suggests that the Co^{2+}/Co^{3+}(FK209) rather than the I^-/I_3^- redox couple participates in the hole conduction (reactions [6[and [7]) in the Co-DSCs.

$$2Co^{2+}(FK209) + 2Dye^{+} \rightarrow 2Co^{3+}(FK209) + 2Dye \quad (6)$$

$$2Co^{3+}(FK209) + 2e^{-}(Pt) \rightarrow 2Co^{2+}(FK209) \quad (7)$$

Through the addition of MXene, a substantial enhancement of the J_{sc} and a slight decrement in the V_{oc} values were observed in the Co-DSCs with $Ti_3C_2T_x$ when compared with those of the reference cell without MXene, as shown in Figure 1a,b, respectively. There was no meaningful variation in the *FF* value, as demonstrated in Figure 1c. As a consequence, an improvement in the PCE was recorded in the MXene-incorporated Co-DSCs because the increase in the J_{sc} overcame the decrement in the V_{oc} value, as shown in Figure 1d. Among the four cells, we focused on the best-performing cells to reveal the origins of the improvement in the PCE via the incorporation of $Ti_3C_2T_x$ MXene into Co^{3+}/I^- liquid redox mediators. Here, we denote the best-performing Co-DSCs with or without $Ti_3C_2T_x$ MXene as $Ti_3C_2T_x$-Co-$_b$DSC or bare Co-$_b$DSC, respectively. Figure 2 presents the current density–voltage (*J–V*) curves of the $Ti_3C_2T_x$- and bare Co-$_b$DSC, while the cell performance is compared in Table 3.

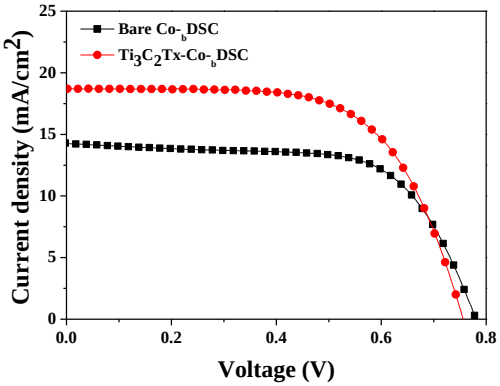

Figure 2. *J–V* characteristics of the best-performing cells—that is, the bare Co-$_b$DSC and $Ti_3C_2T_x$-Co-$_b$DSC.

Table 3. Photovoltaic performance of the best-performing cells—that is, the bare Co-$_b$DSC and $Ti_3C_2T_x$-Co-$_b$DSC.

Best-performing cells	J_{sc} (mA/cm²)	V_{oc} (V)	*FF* (%)	PCE (%)
Bare Co-$_b$DSC	14.41	0.780	64.66	7.27
$Ti_3C_2T_x$-Co-$_b$DSC	18.45	0.760	64.23	9.01

2.2. Effects of $Ti_3C_2T_x$ Incorporation on the J_{sc} of Co-DSCs

Through the incorporation of $Ti_3C_2T_x$ MXene into the Co^{3+}/I^- redox mediator, the J_{sc} value (18.45 mA/cm²) of the $Ti_3C_2T_x$-Co-$_b$DSC was substantially improved from that of the bare Co-$_b$DSC (14.41 mA/cm²). It is believed that the conductive $Ti_3C_2T_x$ MXene present in the Co^{2+}/Co^{3+}(FK209) electrolyte reduced the charge transfer resistance and improved the electrocatalytic performance between the Co^{3+}(FK209) and the platinized FTO electrode, thereby leading to a reduction in the internal resistances and, therefore, an increase in the J_{sc} value of the $Ti_3C_2T_x$-Co-$_b$DSC [21,22,27]. To confirm this, impedance spectroscopic (EIS) analysis was performed for the bare and $Ti_3C_2T_x$-Co-$_b$DSC. Figure 3a shows the Nyquist plots of the EIS spectra of the Co-DSCs, as measured at the open-circuit condition under under AM 1.5 one-sun illumination, providing the series (R_s) and internal

 doi:10.20944/preprints202402.1201.v1

resistances. Three typical arcs, corresponding to the resistance (R_1) of the redox reaction at the platinized FTO/electrolyte interface in the high-frequency region, the electron transfer resistance (R_2) at the TiO_2/dye/electrolyte interface in the medium-frequency region, and the ionic diffusion resistance (R_3) within the electrolyte, were observed. A smaller R_1 value (around 3.18 Ω) was measured in the $Ti_3C_2T_x$-Co-$_b$DSC when compared with that of the bare Co-$_b$DSC (around 4.11 Ω). This indicates that the incorporation of $Ti_3C_2T_x$ MXene can lead to an improvement in the electrocatalytic performance, causing an increase in the hole collection efficiency, when considering that the R_1 value is related to the reduction of the Co^{3+}(FK209) by the Pt catalyst (chemical reaction [7]) [21,22,27]. In addition, it is considered that the reduced resistance (R_1) associated with chemical reaction (7) can effectively produce Co^{2+}(FK209), resulting in the promotion of dye regeneration (chemical reaction [6]) [27].

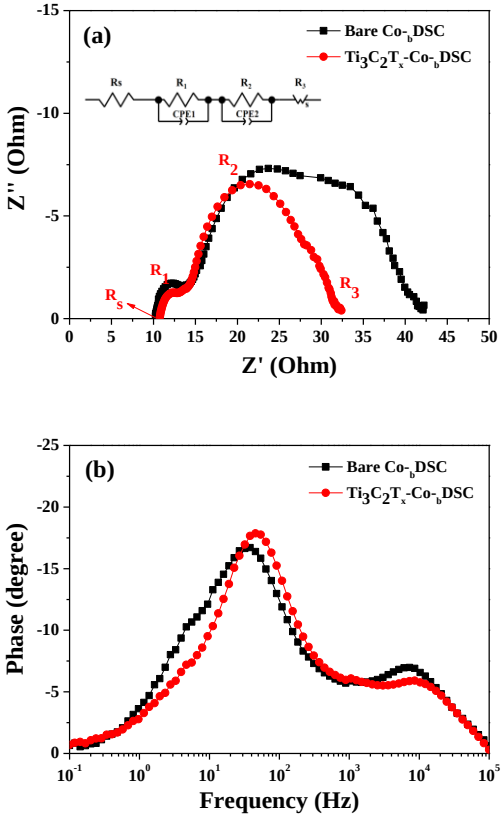

Figure 3. Nyquist (**a**) and Bode (**b**) plots of the EIS spectra for the bare- and $Ti_3C_2T_x$-Co-$_b$DSCs, as measured under open-circuit conditions and under the illumination of simulated AM 1.5 solar light.

Furthermore, a shift in the TiO_2's CBE could be estimated from the dark current curves of the DSCs [28–30]. Figure 4 presents the dark current–voltage curves of the bare- and $Ti_3C_2T_x$-Co-$_b$DSCs. The onset potential of the dark current for the bare Co-$_b$DSC was estimated to be approximately 0.771 V, whereas the onset potential for the $Ti_3C_2T_x$-Co-$_b$DSC was shifted to approximately 0.661 V. Through the incorporation of $Ti_3C_2T_x$ MXene, a lower onset potential was recorded, indicating that the potential difference between the work function of the FTO and the TiO_2's CBE in the $Ti_3C_2T_x$-Co-$_b$DSC was smaller than that in the bare Co-$_b$DSC. This suggests that the TiO_2's CBE in the $Ti_3C_2T_x$-Co-$_b$DSC was located at a more positive potential than that in the bare Co-$_b$DSC. It is thought that **the** $Ti_3C_2T_x$ MXene particles are adsorbed on the TiO_2 surface, causing a surface dipole to be formed and resulting in a positive shift in the TiO_2's CBE. This positive shift (away from the vacuum level) of the CBE in the $Ti_3C_2T_x$-Co-$_b$DSC may lead to the more favorable injection of photoexcited electrons from the dye into the TiO_2 due to the larger potential difference between the dye's lowest unoccupied molecular orbital level and the TiO_2's CBE, thereby resulting in an improvement in the electron injection efficiency [31]. Thus, it is considered that the more positive shift of the TiO_2's CBE in the

 doi:10.20944/preprints202402.1201.v1

$Ti_3C_2T_x$-Co-$_b$DSC yielded a higher electron injection efficiency than the bare Co-$_b$DSC. A similar result was reported in relation to the incorporation of $Ti_3C_2T_x$ MXene into the mesoporous TiO_2 layer, which induced a positive shift in the TiO_2's CBE, leading to an enhancement of the electron injection efficiency [32]. Overall, we attributed the enhanced J_{sc} value in the $Ti_3C_2T_x$-Co-$_b$DSC to the increases in both the hole collection and the dye-regeneration efficiency, which resulted from the reduced internal resistances, as well as to the improvement in the electron injection efficiency due to the positive shift of the TiO_2's CBE.

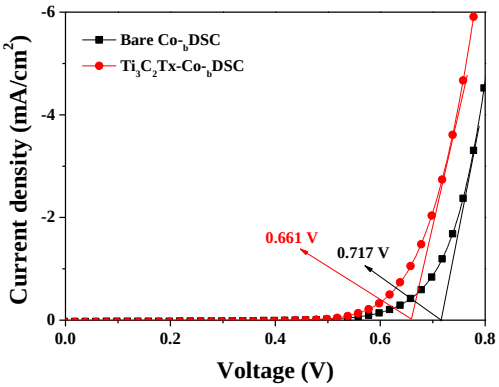

Figure 4. Dark current curves of the best-performing cells—that is, bare Co-$_b$DSC and $Ti_3C_2T_x$-Co-$_b$DSC.

2.3. Effects of $Ti_3C_2T_x$ Incorporation on the V_{oc} of Co-DSCs

The V_{oc} value (0.760 V) of the $Ti_3C_2T_x$-Co-$_b$DSC was decreased when compared with that of the bare Co-$_b$DSC (0.780 V). As expressed in Equation (8), the V_{oc} value of the DSCs under constant illumination can be expressed as a function of the quasi-Fermi level (E_{Fn}) and the dark value (E_{F0}), which is related to the thermal energy (k_BT; 4.11 × 10^{-21} J at 25°C), Boltzmann constant (k_B), absolute temperature (T), positive elementary charge (e; 1.602 × 10^{-19} C), concentration in the dark (n_0), and free electron density of the TiO_2 photoelectrode (n) [33–35]. Equation (8) indicates that the V_{oc} is affected by n, which is closely related to the back electron transfer (BET) reaction that occurs between the photoinjected electrons and the ions in the electrolyte. As the BET reaction decreases the n value, suppression of the BET reaction is necessary to increase the V_{oc}. The n value can be estimated by measuring the lifetime of the electrons photoinjected into the TiO_2, where a longer electron lifetime can increase the n value and, therefore, the V_{oc}. Figure 3b shows Bode phase plots of the EIS spectra of the bare and $Ti_3C_2T_x$-Co-$_b$DSCs. Using the peak frequencies (f_{max}) of 38.2 Hz and 45.5 Hz obtained from the EIS Bode phase plots of the bare and $Ti_3C_2T_x$-Co-$_b$DSCs, respectively, the electron lifetime (τ_n) was estimated using Equation (9) [29,36]. The calculated electron lifetimes were 4.16 ms and 3.50 ms for the bare and $Ti_3C_2T_x$-Co-$_b$DSCs, respectively. A shortened lifetime on the part of the electrons injected from the photoexcited dyes was observed for the $Ti_3C_2T_x$-Co-$_b$DSC relative to that of the control cell (bare Co-$_b$DSC), indicating that the BET reaction (chemical reaction [10]) in the $Ti_3C_2T_x$-Co-$_b$DSC occurred faster than that in the bare Co-$_b$DSC.

$$V_{OC} = \frac{E_{Fn} - E_{F0}}{e} = \frac{k_B T}{e} \ln\left(\frac{n}{n_0}\right) \quad (8)$$

$$\tau_n = \frac{1}{2\pi f_{max}} \quad (9)$$

$$Co^{3+}(FK209) + e^- (TiO_2) \rightarrow Co^{2+}(FK209) \quad (10)$$

To further confirm that the BET reaction was faster in the $Ti_3C_2T_x$-Co-$_b$DSC, Nyquist plots of the EIS spectra measured at −0.7 V in the dark were obtained, as shown in Figure 5a. When the EIS measurement is performed in the dark, electrons are injected from the FTO into the TiO_2 under external applied voltage and then transferred to the electrolyte. Thus, the R_2′ value of the Nyquist plot measured in the dark corresponds to the resistance of the BET reaction between the Co^{3+}(FK209) in the electrolyte and the electrons injected into the TiO_2 conduction band (reaction [10]). It was observed that the arc of the impedance component R_2′ in the $Ti_3C_2T_x$-Co-$_b$DSC was smaller than that

 doi:10.20944/preprints202402.1201.v1

in the bare Co-$_b$DSC. The smaller semicircle in the R_2' suggests that the BET reaction at the TiO_2/dye/electrolyte interface was faster [34,35]. Moreover, from the peak frequencies (f_{max}) given in Figure 5b and Equation (9), the lifetime of the electrons injected from the FTO was calculated to be 11.9 ms and 8.4 ms for the bare and $Ti_3C_2T_x$-Co-$_b$DSCs, respectively. The same tendency in terms of a shortened electron lifetime was observed in the measurements under illumination (Figure 3b) and dark conditions (Figure 5b). Overall, a faster BET reaction resulted in a lower n value, leading to a decrease in the V_{oc} of the $Ti_3C_2T_x$-Co-$_b$DSC based on Equation (8). Furthermore, the reduced V_{oc} value in the $Ti_3C_2T_x$-Co-$_b$DSC can be explained by the positive shift in the TiO_2's CBE, as discussed above (Figure 4). The lower n value can cause the positioning of the TiO_2's CBE to shift in a positive direction, lowering the V_{oc} value due to the narrower potential gap between the TiO_2's CBE and the redox potential of the electrolyte [39,40]. It is considered that this decrease in the V_{oc} (or n) value originated from the adsorption of the $Ti_3C_2T_x$ MXene on the TiO_2 surface. More specifically, the electronically conductive $Ti_3C_2T_x$ MXene particles could provide pathways for chemical reaction (10)—that is, the BET reaction between the photoinjected electrons and the Co^{3+}(FK209) in the redox mediator.

As a reference, the shorter electron lifetime observed in the $Ti_3C_2T_x$-Co-$_b$DSC may decrease the electron collection on the FTO and, therefore, the J_{sc} value. In this study, it is believed that the enhanced hole collection, dye regeneration, and electron injection efficiencies surpassed the decreased electron collection efficiency.

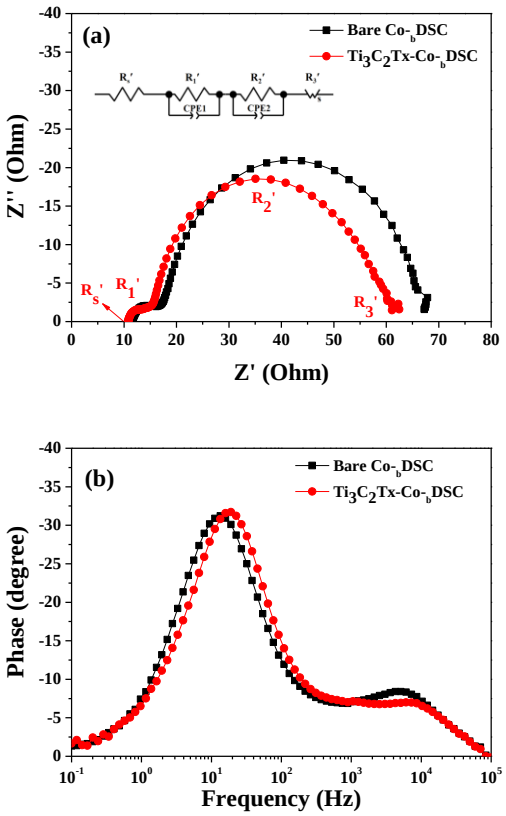

Figure 5. Nyquist (a) and Bode (b) plots of the EIS spectra for the bare- and $Ti_3C_2T_x$-Co-$_b$DSCs, as measured at −0.7 V in the dark.

2.4. Long Long-Term Stability of the Bare- and $Ti_3C_2T_x$-Co-$_b$DSCs

We compared the long-term stability of the bare- and $Ti_3C_2T_x$-Co-$_b$DSCs by evaluating their photovoltaic properties over time. Here, the fabricated devices were additionally sealed using hot-melt glue sticks to minimize the electrolyte leakage. Prior to the measurement of the photovoltaic performance, the I-DSCs with or without $Ti_3C_2T_x$ MXene were converted into Co-DSCs through exposing them to the AM 1.5 condition for 150 min. Figure 6 compares the time-dependent performance variations of the cells stored at room temperature in the dark. Similar decay curves were

 doi:10.20944/preprints202402.1201.v1

noted in both devices, indicating that the incorporation of $Ti_3C_2T_x$ MXene into the redox mediator did not affect the devices' stability.

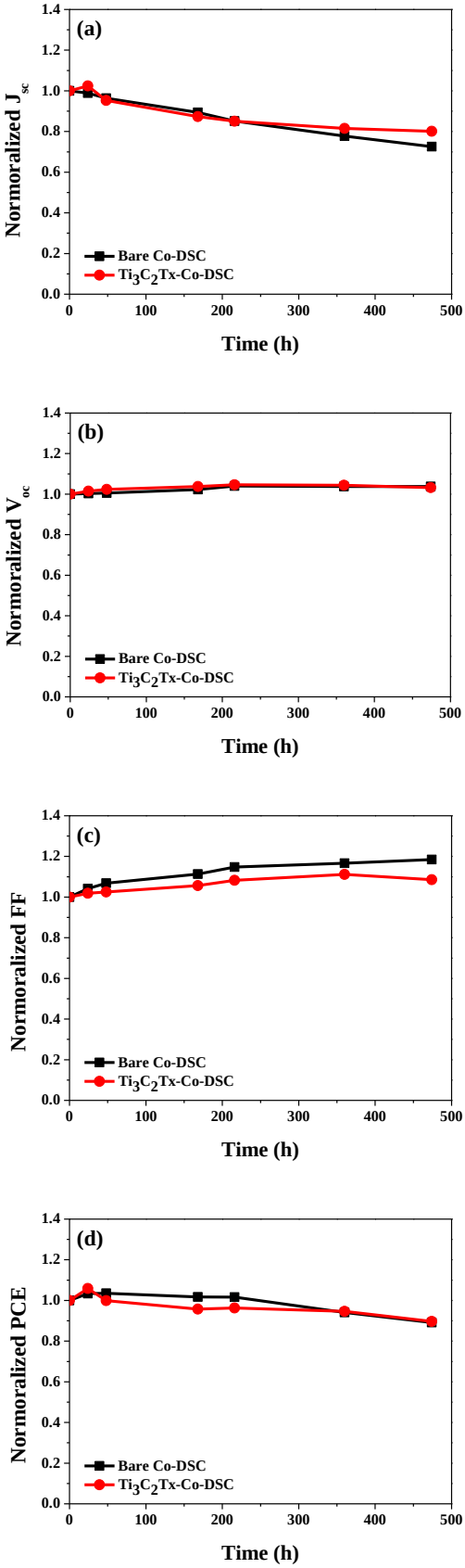

Figure 6. Variations in the photovoltaic performance over time: normalized J_{sc} (a), V_{oc} (b), *FF* (c) and PCE (d) of the bare- and $Ti_3C_2T_x$-Co-bDSCs stored at room temperature in the dark.

 doi:10.20944/preprints202402.1201.v1

3. Materials and Methods

3.1. Materials

To fabricate DSCs, the same materials as those used in our previous report were utilized [23]. Detailed their information is provided in the ESI. The acetonitrile solvent used to prepare the liquid electrolytes was procured from Daejung Chemicals and Metals Co., Ltd. (Gyeonggi-do, Korea). Colloidal suspension of single-layer Ti_3C_2 in acetonitrile (2 mg Ti_3C_2/mL) (BK2020082105-08) was purchased from Beijing Beike New Material Technology Co., Ltd. (Jiangsu, China). All the chemicals used for DSC fabrication were exploited without further purification. The single-layer Ti_3C_2Tx MXene structure is illustrated in Figure S2 in the ESI. The chemical structures of the main components (FK209 and MPII) and additives (LiTFSI and TBP) of the electrolyte are shown in Figure S3 in the ESI.

3.2. Preparation of Co^{3+}/I^--Based Liquid Electrolytes with or without $Ti_3C_2T_x$

The $Ti_3C_2T_x$-dispersed liquid electrolyte based on a Co^{3+}/I^- redox mediator was prepared by dissolving MPII (0.6 M, 302.5 mg), FK209 (0.015 M, 15.2 mg), TBP (0.11 M, 32.4 mg), and LiTFSI (0.04 M, 22.8 mg) in the single-layer Ti_3C_2Tx colloid (2 ml). For the purpose of comparison, Co^{3+}/I^--based liquid electrolytes without Ti_3C_2Tx were also prepared by simply replacing the Ti_3C_2Tx colloid with acetonitrile solvent (2 ml).

3.3. Fabrication of DSCs

Similar procedures to those described in our previous work were utilized to prepared the working (glass/FTO/TiO_2:dye) and counter (glass/FTO/Pt) electrodes for the DSCs [23]. A 60-μm-thick hot-melt adhesive was placed between the working and counter electrodes and then annealed for 10 min at 120 °C to seal the two electrodes. The Co^{3+}/I^--based liquid electrolytes with or without $Ti_3C_2T_x$ MXene were injected into the cells through one of the two small holes predrilled into the counter electrodes. By sealing the two holes, we were able to fabricate DSCs with a 25 mm^2 active area. Detailed procedures are mentioned in the ESI.

3.4. Measurements

Photovoltaic performance measurements, EIS analyses and dark current studies were carried out. All the measurements were performed under ambient conditions at room temperature. Detailed information for the measuring instruments is presented in the ESI.

4. Conclusions

The photovoltaic properties of DSCs with or without Ti_3C_2Tx MXene in Co^{3+}/I^--based redox mediators were investigated in this study. Through the incorporation of $Ti_3C_2T_x$ MXene into the Co^{3+}/I^- liquid redox mediators, the average J_{sc} value of the I-DSCs, in which hole conduction occurred via the redox reaction of the I^- and I_3^- ions, was enhanced, whereas the average V_{oc} value was decreased when compared with that of the device without the MXene. As a result, the average PCE of the I-DSCs with $Ti_3C_2T_x$ was very similar to that of the cells without $Ti_3C_2T_x$. To obtain Co-DSCs based on the Co^{2+}/Co^{3+} redox couple, the I-DSCs were exposed to light for 150 min. Through the addition of Ti_3C_2Tx MXene into the Co^{3+}/I^--based redox mediators, the hole collection, dye regeneration, and electron injection efficiencies of the Ti_3C_2Tx-Co-DSCs were all increased, leading to an improvement in both the J_{sc} and PCE when compared with those of the bare Co-DSCs without MXene. These results indicate that Ti_3C_2Tx MXene, as a J_{sc}-improver, is a good additive for improving the PCE of Co-DSCs.

Supplementary Materials: The following supporting information can be downloaded at: www.mdpi.com/xxx/s1, Table S1: Photovoltaic parameters of I- and Co-DSCs with or without $Ti_3C_2T_x$ MXene; Figure S1: Improvement in V_{oc} values by exposing I-DSCs to AM 1.5 light; Figure S2: Illustration of single-

layered Ti_3C_2Tx MXene structure; Figure S3. Chemical structures of (a) FK209, (b) MPII, (c) LiTFSI, and (d) TBP.

Author Contributions: Conceptualization, Y.S.H.; methodology, Y.S.H. and K.-H.J.; formal analysis, J.H.G. and D.P.; writing—original draft preparation, Y.S.H.; writing—review and editing, K.-H.J. and B.-C.L.; funding acquisition, Y.S.H. and K.-H.J. All authors have read and agreed to the published version of the manuscript.

Funding: Please add: This work was supported by the National Research Foundation of Korea (NRF) grant funded by the Korean government (MSIT) (No. NRF-2022R1A2C1003512). This research was also funded by "Regional Innovation Strategy (RIS)" through the National Research Foundation of Korea (NRF) funded by the Ministry of Education (MOE) (2022RIS-006).

Data Availability Statement: Data are contained within the article and the supplementary material.

Conflicts of Interest: The authors declare no conflict of interest. The funders had no role in the design of the study; in the collection, analyses, or interpretation of data; in the writing of the manuscript; or in the decision to publish the results.

References

1. Naguib, M.; Kurtoglu, M.; Presser, V.; Lu, J.; Niu, J.; Heon, M.; Hultman, L.; Gogotsi, Y. Two-dimensional nanocrystals produced by exfoliation of Ti_3AlC_2. *Adv. Mater.* **2011**, *23*, 4248–4253. https://doi.org/10.1002/adma.201102306.
2. Papadopoulou, K.A.; Chroneos, A.; Parfitt, D.; and Christopoulos, S.-R.G. A perspective on MXenes: their synthesis, properties, and recent applications. *J. Appl. Phys.* **2020**, *128*, 170902. https://doi.org/10.1063/5.0021485.
3. Jun, B.-M.; Kim, S.; Heo, J.; Park, C.M.; Her, N.; Jang, M.; Huang, Y.; Han, J.; Yoon, Y. Review of MXenes as new nanomaterials for energy storage/delivery and selected environmental applications. *Nano Res.* **2019**, *12*, 471–487. https://doi.org/10.1007/s12274-018-2225-3.
4. Jimmy, J.; Kandasubramanian, B. MXene functionalized polymer composites: synthesis and applications. *Eur. Polym. J.* **2020**, *122*, 109367. https://doi.org/10.1016/j.eurpolymj.2019.109367.
5. Saeed, M.A.; Shahzad, A.; Rasool, K.; Mateen, F.; Oh, J.-M.; Shim, J.W. 2D MXene: a potential candidate for photovoltaic cells? a critical review. *Adv. Sci.* **2022**, *9*, 2104743. https://doi.org/10.1002/advs.202104743.
6. Yin, L.; Li, Y.; Yao, X.; Wang, Y.; Jia, L.; Liu, Q.; Li, J.; Li, Y.; He, D. MXenes for solar cells. *Nano-Micro Lett.* **2021**, *13*, 78. https://doi.org/10.1007/s40820-021-00604-8.
7. Shi, Z.; Khaledialidusti, R.; Malaki, M.; Zhang, H. MXene-based materials for solar cell applications. *Nanomaterials* **2021**, *11*, 3170. https://doi.org/10.3390/nano11123170.
8. Qamar, S.; Fatima, K.; Ullah, N.; Akhter, Z.; Waseem, A.; Sultan, M. Recent progress in use of MXene in perovskite solar cells: for interfacial modification, work-function tuning, and additive engineering. *Nanoscale* **2022**, *14*, 13018–13039. https://doi.org/10.1039/d2nr02799b.
9. Di, Y.; Qin, T. Efficient wide-spectrum dye-sensitized solar cell by plasmonic TiN@Ni-MXene as electrocatalyst. *Ceram. Int.* **2022**, *48*, 12635–12640. https://doi.org/10.1016/j.ceramint.2022.01.132.
10. Ma, J.-Y.; Sun, M.; Zhu, Y.-A.; Zhou, H.; Wu, K.; Xiao, J.; Wu, M. Highly effective 2D layer structured titanium carbide electrode for dye-sensitized and perovskite solar cells. *ChemElectroChem* **2020**, *7*, 1149–1154. https://doi.org/10.1002/celc.201902159.
11. Nagalingam, S.P.; Grace, A.N. Poly(3,4-ethylenedioxythiophene) decorated MXene as an alternative counter electrode for dye-sensitized solar cells. *Mater. Today Chem.* **2022**, *26*, 101113. https://doi.org/10.1016/j.mtchem.2022.101113.
12. Chen, T.; Tong, G.; Xu, E.; Li, H.; Li, P.; Zhu, Z.; Tang, J.; Qi, Y.; Jiang, Y. Accelerating hole extraction by inserting 2D Ti_3C_2-MXene interlayer to all inorganic perovskite solar cells with long-term stability. *J. Mater. Chem. A* **2019**, *7*, 20597–20603. https://doi.org/10.1039/c9ta06035a.
13. Jin, X.; Yang, L.; Wang, X.-F. Efficient two-dimensional perovskite solar cells realized by incorporation of $Ti_3C_2T_x$ MXene as nano-dopants. *Nano-Micro Lett.* **2021**, *13*, 68. https://doi.org/10.1007/s40820-021-00602-w.
14. Agresti, A.; Pazniak, A.; Pescetelli, S.; Di Vito, A.; Rossi, D.; Pecchia, A.; Auf der Maur, M.; Liedl, A.; Larciprete, R.; Kuznetsov, D.V.; Saranin, D.; Di Carlo, A. Titanium-carbide MXenes for work function and interface engineering in perovskite solar cells. *Nat. Mater.* **2019**, *18*, 1228–1234. https://doi.org/10.1038/s41563-019-0478-1.

15. Hou, C.; Yu, H. Modifying the nanostructures of PEDOT:PSS/$Ti_3C_2T_x$ composite hole transport layers for highly efficient polymer solar cells. *J. Mater. Chem. C* **2020**, *8*, 4169–4180. https://doi.org/10.1039/D0TC00075B.
16. Hou, C.; Yu, H.; Huang, C. Solution-processable $Ti_3C_2T_x$ nanosheets as an efficient hole transport layer for high-performance and stable polymer solar cells. *J. Mater. Chem. C* **2019**, *7*, 11549–11558. https://doi.org/10.1039/C9TC03415C.
17. Gong, J.; Sumathya, K.; Qiao, Q.; Zhou, Z. Review on dye-sensitized solar cells (DSSCs): advanced techniques and research trends. *Renew. Sustain. Energy Rev.* **2017**, *68*, 234–246. https://doi.org/10.1016/j.rser.2016.09.097.
18. Sharma, K.; Sharma, V.; Sharma, S.S. Dye-sensitized solar cells: fundamentals and current status. *Nanoscale Res. Lett.* **2018**, *13*, 381. https://doi.org/10.1186/s11671-018-2760-6.
19. Wu, J.; Lan, Z.; Lin, J.; Huang, M.; Huang, Y.; Fan, L.; Luo, G. Electrolytes in dye-sensitized solar cells. *Chem. Rev.* **2015**, *115*, 2136–2173. https://doi.org/10.1021/cr400675m.
20. Iftikhar, H.; Sonai, G.G.; Hashmi, S.G.; Nogueira, A.F.; Lund, P.D. Progress on electrolytes development in dye-sensitized solar cells. *Materials* **2019**, *12*, 1998. https://doi.org/10.3390/ma12121998.
21. Wen, J.; Liu, Y.; Li, T.; Liu, C.; Wang, T.; Liu, Y.; Zhou, Y.; Li, G.; Sun, Z. Low cost and strongly adsorbed melamine formaldehyde sponge electrolyte for nontraditional quasi-solid dye-sensitized solar cells. *ACS Appl. Energy Mater.* **2023**, *6*, 4952–4960. https://doi.org/10.1021/acsaem.3c00382.
22. Wen, J.; Sun, Z.; Qiao, Y.; Zhou, Y.; Liu, Y.; Zhang, Q.; Liu, Y.; Jiao, S. Ti_3C_2 MXene-reduced graphene oxide composite polymer-based printable electrolyte for quasi-solid-State dye-sensitized solar cells. *ACS Appl. Energy Mater.* **2022**, *5*, 3329–3338. https://doi.org/10.1021/acsaem.1c03928.
23. Lee, Y.; Kwon, Y.; Cho, Y.; Ahn, K.-S.; Han, Y.S. Novel heterologous binary redox mediator based on an ionic liquid and cobalt complex for efficient organic-solvent-free dye-sensitized solar cells. *J. Ind. Eng. Chem.* **2022**, *115*, 263–271. https://doi.org/10.1016/j.jiec.2022.08.007.
24. Noh, J.H.; Jeon, N.J.; Choi, Y.C.; Nazeeruddin, M.K.; Grätzel, M.; Seok, S.I. Nanostructured TiO_2/$CH_3NH_3PbI_3$ heterojunction solar cells employing spiro-OMeTAD/Co-complex as hole-transporting material. *J. Mater. Chem. A* **2013**, *1*, 11842–11847. https://doi.org/10.1039/c3ta12681a.
25. Zhang, Y.; Sun, Z.; Shi, C.; Yan, F. Highly efficient dye-sensitized solar cells based on low concentration organic thiolate/disulfide redox couples. *RSC Adv.* **2016**, *6*, 70460–70467. https://doi.org/10.1039/c6ra11592f.
26. Xu, D.; Zhang, H.; Chen, X.; Yan, F. Imidazolium functionalized cobalt tris(bipyridyl) complex redox shuttles for high efficiency ionic liquid electrolyte dye-sensitized solar cells. *J. Mater. Chem. A* **2013**, *1*, 11933–11941. https://doi.org/10.1039/c3ta12031g.
27. Chen, X.; Tang, Q.; He, B.; Lin, L.; Yu, L. Platinum-free binary Co-Ni alloy counter electrodes for efficient dye-sensitized solar cells. *Angew. Chem.* **2014**, *126*, 10975–10979. https://doi.org/10.1002/ange.201406982.
28. Diamant, Y.; Chen, S.G.; Melamed, O.; Zaban, A. Core-shell nanoporous electrode for dye sensitized solar cells: the effect of the $SrTiO_3$ shell on the electronic properties of the TiO_2 core. *J. Phys. Chem. B* **2003**, *107*, 1977–1981. https://doi.org/10.1021/jp027827v.
29. Baek, G.W.; Kim, Y.-J.; Jung, K.-H.; Han, Y.S. Enhancement of solar cell performance through the formation of a surface dipole on polyacrylonitrile-treated TiO_2 photoelectrodes. *J. Ind. Eng. Chem.* **2019**, *73*, 260–267. https://doi.org/10.1016/j.jiec.2019.01.036.
30. Shin, S.; Kim, J.; Kwon, S.-J.; Ryu, K.H.; Choi, B.; Han, Y.S. Enhancement of photovoltaic performance of solvent-free dye-sensitized solar cells with doped poly(3-hexylthiophene). *J. Ind. Eng. Chem.* 2023, *123*, 428–435. https://doi.org/10.1016/j.jiec.2023.03.060.
31. Watson, D.F.; Meyer, G.J. Cation effects in nanocrystalline solar cells. *Coord. Chem. Rev.* **2004**, *248*, 1391–1406. https://doi.org/10.1016/j.ccr.2004.02.015.
32. Lemos, H.G.; Ronchi, R.M.; Portugal, G.R.; Rossato, J.H.H.; Selopal, G.S.; Barba, D.; Venancio, E.C.; Rosei, F.; Arantes, J.T.; Santos, S.F. Efficient $Ti_3C_2T_x$ MXene/TiO_2 hybrid photoanodes for dye-sensitized solar cells. *ACS Appl. Energy Mater.* **2022**, *5*, 15928–15938. https://doi.org/10.1021/acsaem.2c03474.
33. Peng, T.; Shi, W.; Wu, S.; Ying, Z.; Ri, J.H. Sea urchin-like TiO_2 microspheres as scattering layer of nanosized TiO_2 film-based dye-sensitized solar cell with enhanced conversion efficiency. *Mater. Chem. Phys.* **2015**, *164*, 238–245. https://doi.org/10.1016/j.matchemphys.2015.08.054.
34. Zaban, A.; Greenshtein, M.; Bisquert, J. Determination of the Electron lifetime in nanocrystalline dye solar cells by open-circuit voltage decay measurements. *ChemPhysChem* **2003**, *4*, 859–864. https://doi.org/10.1002/cphc.200200615.
35. Kim, J.Y.; Kim, K.H.; Kim, D.-H.; Han, Y.S. Effects of a dianion compound as a surface modifier on the back reaction of photogenerated electrons in TiO_2-based solar cells. *Arabian J. Chem.* **2020**, *13*, 2340–2348. https://doi.org/10.1016/j.arabjc.2018.04.017.
36. Kim, K.S.; Song, H.; Nam, S.H.; Kim, S.-M.; Jeong, H.; Kim, W.B.; Jung, G.Y. Fabrication of an efficient light-scattering functionalized photoanode using periodically aligned ZnO hemisphere crystals for dye-sensitized solar cells. *Adv. Mater.* **2012**, *24*, 792–798. https://doi.org/10.1002/adma.201103985.

 doi:10.20944/preprints202402.1201.v1

37. Zhao, J.; Sun, B.; Qiu, L.; Cao, H.; Li, Q.; Chen, X.; Yan, F. Efficient light-scattering functionalized TiO_2 photoanodes modified with cyanobiphenyl-based benzimidazole for dye-sensitized solar cells with additive-free electrolytes. *J. Mater. Chem.* **2012**, *22*, 18380–18386. https://doi.org/10.1039/c2jm32607h.
38. Tian, H.; Hu, L.; Zhang, C.; Liu, W.; Huang, Y.; Mo, L.; Guo, L.; Sheng, J.; Dai, S. Retarded charge recombination in dye-sensitized nitrogen-doped TiO_2 solar cells. *J. Phys. Chem. C* **2010**, *114*, 1627–1632. https://doi.org/10.1021/jp9103646.
39. Park, K.-H.; Dhayal, M. High efficiency solar cell based on dye sensitized plasma treated nano-structured TiO_2 films. *Electrochem. Commun.* **2009**, *11*, 75–79. https://doi.org/10.1016/j.elecom.2008.10.020.
40. Mandal, D.; Hamann, T.W. Charge distribution in nanostructured TiO_2 photoanode determined by quantitative analysis of the band edge unpinning. *ACS Appl. Mater. Interfaces* **2016**, *8*, 419–424. https://doi.org/10.1021/acsami.5b09200.